Near-Infrared Raman Spectroscopy for *in Vivo* Detection of Cervical Precancers

URS UTZINGER, DOUGLAS L. HEINTZELMAN, ANITA MAHADEVAN-JANSEN, ANAIS MALPICA, MICHELE FOLLEN, and REBECCA RICHARDS-KORTUM*

The Biomedical Engineering Program, The University of Texas at Austin, Austin, Texas 78712 (U.U., D.L.H., R.R.-K.); Department of Biomedical Engineering, Vanderbilt University, Nashville, Tennessee (A.M.-J.); Department of Pathology, The University of Texas M.D. Anderson Cancer Center, Houston, Texas 77030 (A.M.); and Department of Gynecology Oncology, The University of Texas M.D. Anderson Cancer Center, Houston, Texas 77030 and Department of Obstetrics, Gynecology and Reproductive Health Sciences, The University of Texas Health Science Center, Houston, Texas 77030 (M.F.)

This study evaluates the potential of near-infrared Raman spectroscopy for *in vivo* detection of squamous dysplasia, a precursor to cervical cancer. A pilot clinical trial was carried out at three clinical sites. Raman spectra were measured from one colposcopically normal and one abnormal area of the cervix. These sites were then biopsied and submitted for routine histologic analysis. Twenty-four evaluable measurements were made *in vivo* in 13 patients. Cervical tissue Raman spectra contain peaks in the vicinity of 1070, 1180, 1195, 1210, 1245, 1330, 1400, 1454, 1505, 1555, 1656, and 1760 cm^{-1}. The ratio of intensities at 1454 to 1656 cm^{-1} is greater for squamous dysplasia than all other tissue types, while the ratio of intensities at 1330 to 1454 cm^{-1} is lower for samples with squamous dysplasia than all other tissue types. A simple algorithm based on these two intensity ratios separates high-grade squamous dysplasia from all others, misclassifying only one sample. Spectra measured *in vivo* resemble those measured *in vitro*. Cervical epithelial cells may contribute to tissue spectra at 1330 cm^{-1}, a region associated with DNA. In contrast, epithelial cells probably do not contribute to tissue spectra at 1454 cm^{-1}, a region associated with collagen and phospholipids.

Index Headings: **Raman spectroscopy; Cervix; *In vivo* study.**

INTRODUCTION

With the advent of molecular medicine, there will be an unprecedented opportunity for interventions based on early detection of disease. Optical technologies offer real-time assessment of biochemical and morphologic tissue composition, and provide an important new tool to improve early detection. Many groups have shown the promise of optical technologies for early detection of numerous pathologies, including atherosclerosis[1,2] and dysplasia.[3,4]

The uterine cervix is a well-established clinical and histopathologic model of cancer progression. Our group has conducted a number of studies to evaluate emerging optical technologies for the *in vivo* detection of cervical dysplasia, including fluorescence spectroscopy,[5] confocal imaging,[6] and optical coherence tomography (OCT).[7] Diagnostic technologies in medicine are compared by using sensitivities, specificities, positive and negative predictive values, and receiver-operator characteristic curves.[8] Emerging optical technologies show promise for cervical precancer detection as measured against traditional technologies such as the Papanicolaou smear and colposcopically directed biopsy, with sensitivities and specificities of optical techniques approaching 80–90% in small and moderate sized clinical trials.[9]

The biological basis of these optical technologies is under intensive study. Reflectance spectroscopy samples electronic-energy-level differences in tissue chromophores, such as hemoglobin and proteins. Fluorescence spectroscopy also is sensitive to electronic-energy-level transitions; native tissue fluorophores include the aromatic amino acids, crosslinks in collagen, and the cofactors NAD(P)H and FAD. Imaging techniques, such as confocal microscopy and OCT, are sensitive to small differences in tissue refractive index. Recently, Raman spectroscopy has been explored as a new diagnostic technique.[10,11] Raman spectroscopy is sensitive to vibrational-energy-level differences. A large number of biological molecules can be probed by using Raman spectroscopy, with many having characteristic fingerprint Raman spectra.

Several investigators have explored the potential of near-infrared Raman spectroscopy for detection of cancer and precancer *in vitro*. Feld and colleagues showed that *in vitro* Raman spectra of normal breast tissue were dominated by peaks characteristic of fatty acids at 1667, 1452, and 1300 cm^{-1} whereas Raman spectra of tumors were dominated by structural protein modes at 1667, 1452, 1260, 890, and 820 cm^{-1}.[12] McCreery and co-workers showed that *in vitro* Raman spectra could classify normal and cancerous breast tissue specimens based on the increased signatures associated with cholesterol and lipid relative to protein.[13] Our group measured Raman spectra of normal and dysplastic cervical tissue *in vitro*; simple but effective algorithms could be developed to discrimi-

Received 27 November 2000; accepted 16 April 2001.
* Author to whom correspondence should be sent.

0003-7028/01/5508-0955$2.00/0

nate dysplasia from normal cervix tissue based on these spectra.[14] As dysplasia developed, the ratio of Raman intensities at 1656 cm^{-1} to that at 1330 cm^{-1} decreased. The ratio of Raman intensities at 1454 cm^{-1} to that at 1656 cm^{-1} was higher for high-grade dysplasias than for low-grade dysplasias. Chromophores that contribute to these Raman peaks include collagen (1454 cm^{-1}, 1656 cm^{-1}), phospholipids (1330 cm^{-1}, 1454 cm^{-1}) and DNA (1330 cm^{-1}). A challenge in these *in vitro* studies was that Raman spectra of biological samples are typically very weak; achieving high signal-to-noise ratios and avoiding background signals produced by the collection optics is difficult.

Achieving a high signal-to-noise ratio and avoiding background signals is even more difficult *in vivo,* because the fiber-optic probes used to collect *in vivo* signals have high Raman signatures in the fingerprint region and integration times and irradiation powers must be limited for practical and safety reasons. Recently, several groups have presented designs for fiber-optic probes that allow measurement of Raman spectra *in vivo.*[15–19] In this study, we present the results of an *in vivo* pilot study using Raman spectroscopy to classify cervical precancer where histopathologic biopsy was used as the gold standard. We then compare these results to our previous *in vitro* work.[14]

Methods. ***Clinical Trial Design.*** A Pap smear is normally obtained by a women's gynecologist or a family physician and analyzed at a cytology laboratory. If results are abnormal, further examination is necessary in a colposcopy clinic where the cervix is examined with a low-power microscope and optical-contrast agents. If abnormal areas are identified they are biopsied and a treatment decision is formed when histological results are available.

The clinical trial was carried out at three sites: The University of Texas M.D. Anderson Cancer Center, the Lyndon Baines Johnson Harris County Health District, and the Hermann Medical Center. Pilot studies at The University of Texas at M.D. Anderson, The University of Texas Health Science Center, and the Harris County Health District Internal Review Boards at the time of the clinical trial allowed for up to 25 patients to be entered into the trial. Each patient was informed of the study and was asked to sign an informed consent. Eligible patients included those referred with the diagnosis of an abnormal Pap smear who were over 18 years old and not pregnant. All patients in the Colposcopy Clinic undergo a complete history and physical examination, sexually transmitted disease screening, a Papanicolaou smear, pan-colposcopy of the vagina, vulva and cervix, and colposcopically directed biopsies of diseased areas.

After the cervical colposcopy, normal and abnormal areas were identified, and Raman spectra were measured from one normal and one abnormal area of the cervix. Each of these sites was then colposcopically biopsied. Biopsies were submitted for routine histologic analysis and read by a gynecologic pathologist. The pathologic categories were normal cervix, inflammation, squamous metaplasia, low-grade squamous dysplasia (HPV and CIN 1), high-grade squamous dysplasia (CIN 2, CIN 3, and CIS), and cancer. The pathologist was blinded to the results of the Raman spectroscopic study.

Instrumentation. Figure 1 shows a block diagram of the system used to collect Raman spectra from cervical epithelium *in vivo.* The system has been described in detail previously.[16] Briefly, it consists of a diode laser at 789 nm coupled to a fiber-optic delivery and collection probe. The probe directs the illumination light onto the cervix and the resulting Raman scattered light onto a holographic spectrograph coupled to a liquid nitrogen cooled, back-illuminated, deep depletion, charge-coupled device (CCD) camera. The probe is optimized to measure epithelial tissue layers because the illumination and collection path cross with an angle of 75° at the tissue site, thus limiting the interrogated tissue volume to the front of the probe. The probe head (12 mm diameter) contains a bandpass filter to remove fluorescence from the excitation path and a holographic notch filter to suppress the reflected excitation light in the collection path.

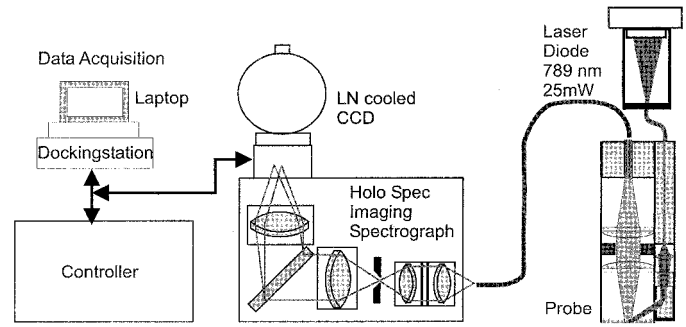

FIG. 1. Block diagram of system used to measure Raman spectra *in vivo.*

The laser output was 15–16.5 mW at the distal end of the fiber-optic probe. Prior to each patient measurement, the probe was disinfected in gluteraldehyde, rinsed in water, and wiped with alcohol. The spectrum of a neon calibration lamp was measured for wavelength calibration purposes. A Raman spectrum was then measured from naphthalene and rhodamine calibration standards. A background spectrum was measured, with the probe covered by a black plastic cap. Finally, the probe was advanced through the speculum and placed in contact with a colposcopically normal and abnormal site on the cervix. Raman spectra were measured from these two sites; integration times ranged from 60 to 180 s. The room light was turned off during measurements or where this was not possible a black cloth covered the pelvis and legs of the patient. Following spectral measurement, each site was biopsied.

Data Processing and Analysis. Signal from the CCD camera was binned along one direction, to create a single spectrum per measurement site. From published neon lines,[20] we identified a subset of 12 lines that were not saturated and detectable in all of the calibration measurements. An automated routine located the neon peaks within a predefined window and fit them to a polynomial function of 2nd degree. This created a relationship between wavelength and pixel number. In a second step, peaks outside an offset of 0.3 nm from the expected location were removed and the same polynomial fit was repeated. This gave a calibration accuracy of approximately 4 cm^{-1} while the spectral resolution was 8 cm^{-1}. For each measurement, wavenumbers were generated based on the center wavelength of the laser emission. Each spectrum was truncated below 1000 cm^{-1}. Cosmic

TABLE I. Histopathologic diagnosis.

Patient number	Colposcopically normal area	Colposcopically abnormal area
9	Squamous metaplasia	High-grade dysplasia
11	Normal	Inflammation
12	Normal	Not measured
15	Normal	Signal-to-noise ratio too low to analyze
16	Normal	Squamous metaplasia
17	Normal	Inflammation
18	Normal	Inflammation
20	Normal	Inflammation
21	Normal	Squamous metaplasia
22	Normal	Low-grade dysplasia
23	Normal	Squamous metaplasia
24	No normal areas available	Two sites–high-grade dysplasia
25	Normal	High-grade dysplasia

rays and defect pixels were removed from the spectra; missing data were replaced with linearly interpolated values between the neighboring pixels.

Each spectrum consisted of a small contribution of Raman scattering atop a large fluorescence background. The fluorescence background varies much more smoothly with wavelength, and thus was removed by using a high-pass Butterworth filter with a cut-off frequency equivalent to 2% of half the sampling frequency.[21] The remaining high-frequency content of the spectrum containing the Raman signal was smoothed with a Savitsky–Golay filter[22] by using a polynomial function of 1st degree and a window width of 5 pixels, which corresponded to the system spectral resolution.

Raman spectra were grouped according to histopathologic findings and average spectra were calculated. These average spectra were examined visually to identify a set of Raman peaks common to most spectra. Then, in the vicinity of these peaks an automated local maxima search routine was applied. Additionally an automated local minima search routine was applied in the same regions. The lowest two local minima on both sides of each local maximum were selected and averaged. The peak intensity was determined by the difference between the local maximum and the average local minimum.

For further analysis, peak intensities were normalized to the common four strongest Raman bands, yielding five datasets: unnormalized peak intensities and four sets of intensity ratios. To identify those peaks and peak ratios corresponding to the most significant differences between tissue types, a student's t-test was applied to test the hypothesis that the mean values of the peak intensities and ratios were different for all types of tissue. For the peaks and ratios with a p-value below 0.1, scatterplots showing pairwise combinations of intensity values and ratios for all samples were plotted. From the two-dimensional scatter plots, linear discriminators were formed relative to the gold standard of histopathology. The number of correctly classified samples was reported. Principal component analysis[14,23] and cross validation techniques were not applied to the data because the sample size was not sufficiently large.[24]

RESULTS

Twenty-five patients consented and entered the study at the combined three sites. The patients ranged in age from 18 to 76 years, and the average age was 32 years. Thrity-six percent were white, 36% were African-American, and 28% were Hispanic. All the patients entered the Colposcopy Clinic with an abnormal Pap smear. Data from the first six patients in the study were excluded from further analysis, as this phase of the study was used to optimize hardware settings. Data from an additional three patients were excluded due to instrument malfunction. Data from one patient was excluded because pathology was unavailable because the histopathologic site location was not recorded. Data from two patients were excluded because interference from room lights resulted in a signal-to-noise ratio of approximately 1. Thus, 24 evaluable measurements were made in 13 patients; the subset of patients excluded differed in no way from those included in further analysis. The results of the histologic biopsies are presented in Table I.

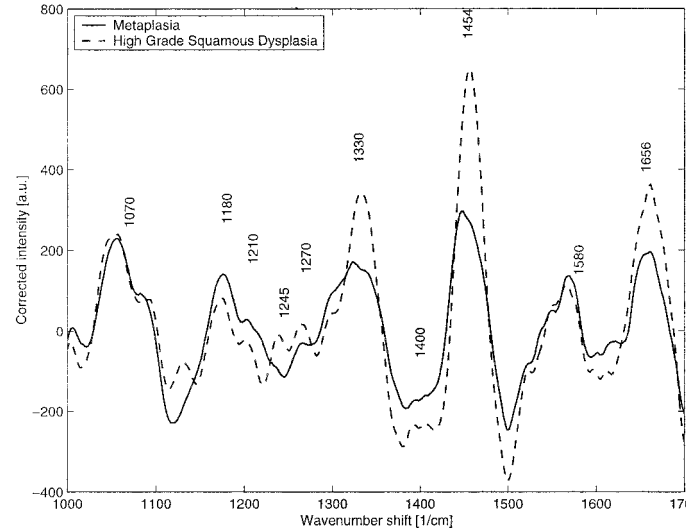

FIG. 2. Typical Raman spectra of a colposcopically normal area of the cervix with metaplasia and a colposcopically abnormal area with high-grade squamous dysplasia.

Figure 2 shows typical processed spectra from patient 9, a patient in whom a colposcopically normal area with histologic evidence of metaplasia (a normal finding in the cervix) is compared to a colposcopically abnormal area with histopathologic diagnosis of high-grade squamous dysplasia. The data-processing method removes the broadband autofluorescence, and in this subtraction process the baseline of the spectrum drops below zero. Because of this, peak intensities are calculated by taking the intensity at the peak and subtracting the intensity at the surrounding minima. Raman peaks are present in the vicinity of 1070, 1180, 1210, 1245, 1270, 1330, 1400, 1454, 1580, and 1656 cm^{-1}. Note that the ratio of intensities at 1454 cm^{-1} to that at 1656 cm^{-1} is higher in the spectrum of the dysplastic sample (1.43) compared to that in the spectrum of the metaplastic sample (1.26). The ratio of intensities at 1656 cm^{-1} to that at 1330 cm^{-1} is decreased in the dysplastic sample (1.23 vs. 1.27), which is consistent with earlier results measured *in vitro*.[14] Also, the ratio of intensities at 1330 cm^{-1} to that at 1454 cm^{-1} is lower in the dysplastic sample (0.56) compared to that in the metaplastic sample (0.63).

Figure 3 shows average spectra for each diagnostic cat-

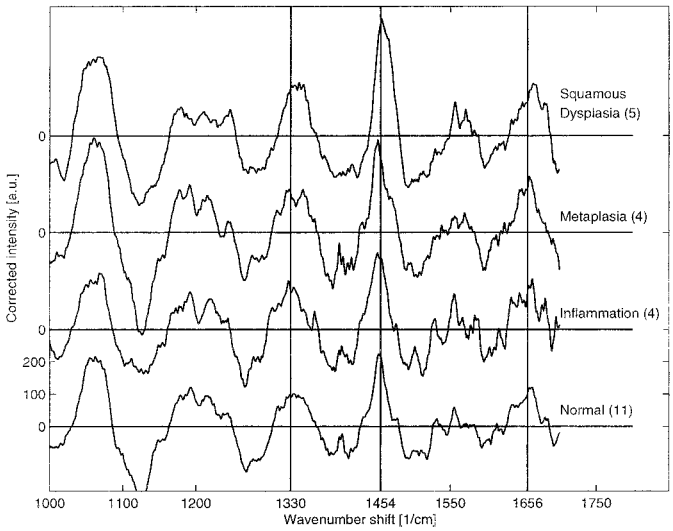

FIG. 3. Average Raman spectra of each diagnostic category. The average intensity ratios at 1454 to 1650 cm^{-1} are higher for squamous dysplasia (2.26) than for normal samples (1.85), samples with inflammation (1.78), and metaplastic samples (1.48). Similarly, the average intensity ratios at 1330 to 1454 cm^{-1} are lower for squamous dysplasias (0.55) than for normal samples (0.60), samples with inflammation (0.72), and metaplastic samples (0.99).

egory: normal, inflammation, metaplasia, and squamous dysplasia. As the diagnosis progresses from normal to inflammation to metaplasia and through squamous dysplasia, the intensity of the Raman peak at 1454 cm^{-1} increases. The intensity of the Raman peaks at 1330 and 1656 cm^{-1} is greater for abnormal samples than normal samples. The ratio of intensities at 1454 to 1656 cm^{-1} is greater on average for squamous dysplasia samples than all other tissue types, while the ratio of intensities at 1330 to 1454 cm^{-1} is lower on average for samples with squamous dysplasia than all other tissue types.

By examining all data we found that Raman peaks are present within 1070 ± 25, 1182 ± 10, 1195 ± 35, 1217 ± 7.5, 1250 ± 7.5, 1330 ± 25, 1400 ± 7.5, 1454 ± 17.5, 1505 ± 7.5, 1555 ± 35, 1656 ± 30, and 1760 ± 20 cm^{-1}. The peaks with the strongest signal were found at 1070, 1330, 1454, and 1656 cm^{-1}. Table II shows the p-values resulting from the statistical comparison of average intensity values at those bands and the intensities normalized to the strongest peaks. Only the intercategory comparisons with p-values less than or equal to 0.05 were included in this table. Note that for differentiating squamous dysplasia from normal tissue, inflammation and metaplasia, ratios of intensities at 1454 to 1656 cm^{-1} and 1330 to 1454 cm^{-1} showed low p-values.

Figure 4 shows diagnostic algorithms derived from these data that correspond to these ratios. This scatterplot indicates the intensity of each of the 24 sites measured by diagnostic category at three frequencies. Figure 4 shows the intensity ratio at 1330/1454 cm^{-1} plotted against the ratio of intensities at 1454/1656 cm^{-1}. The linear discriminator, represented by the straight line, separates high-grade squamous dysplasia from all others, misclassifying only one normal sample.

DISCUSSION AND CONCLUSION

This pilot study shows that it is possible to measure Raman spectra *in vivo* and extract potentially diagnostically useful information. Spectra measured *in vivo* resemble those measured *in vitro*. There are obvious visual differences in the spectra of normal cervix and high-grade squamous dysplasia in the same patient. Average spectra reveal a consistent increase in the Raman intensity at 1330, 1454, and 1650 cm^{-1} as tissue progresses from normal to high-grade squamous dysplasia. These peaks are consistent with contributions from collagen, phospholipids, and DNA. However, because tissue is a complex, heterogeneous structure, definitive assignment is difficult. To assess whether epithelial cell signal contributes to tissue Raman spectra, we measured Raman spectra of a suspension of cervical cancer cells suspended in phosphate buffered saline at a concentration of 10^6 cells per mL with the use of a system described previously.[14] Results are shown in Fig. 5 and indicate that epithelial cells may contribute to tissue spectra at 1330 cm^{-1}, a region associated with DNA. In contrast, epithelial cells probably do not contribute to tissue spectra at 1454 cm^{-1}, a region associated with collagen and phospholipids. A dominating peak for cells in suspension was found at 1656 cm^{-1}. Our results show that intensities at 1330, 1454, and 1656 cm^{-1} can be used to discriminate high-grade squamous

TABLE II. Results of pairwise comparison of average intensities.

Diagnostic category	Wavenumber (cm^{-1})	p-value
Dysplasia vs. inflammation	1182/1070	0.01
Dysplasia vs. inflammation	1400/1070	0.01
Dysplasia vs. metaplasia	1656/1454	0.01
Dysplasia vs. normal	1195/1070	0.02
Dysplasia vs. inflammation	1195/1070	0.02
Dysplasia vs. normal	1454/1656	0.02
Dysplasia vs. inflammation	1454/1656	0.03
Dysplasia vs. metaplasia	1182/1070	0.04
Dysplasia vs. normal	1454/1330	0.04
Dysplasia vs. inflammation	1400/1454	0.04
Dysplasia vs. normal	1182/1454	0.05
Normal vs. inflammation	1760/1070	0.05

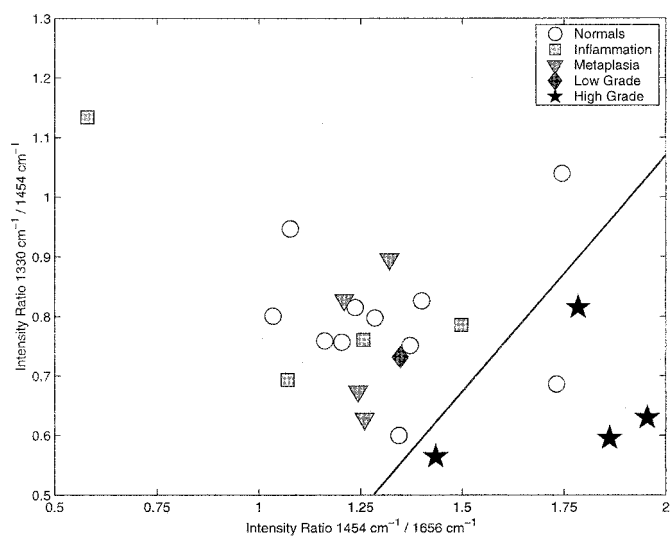

FIG. 4. This scatterplot indicates the intensity of each of the 24 sites measured by diagnostic category at three frequencies; the intensity ratio at 1330/1454 cm^{-1} is plotted against the ratio of intensities at 1454/1656 cm^{-1}. The straight-line algorithm separates high-grade squamous dysplasia from all others, misclassifying one normal sample.

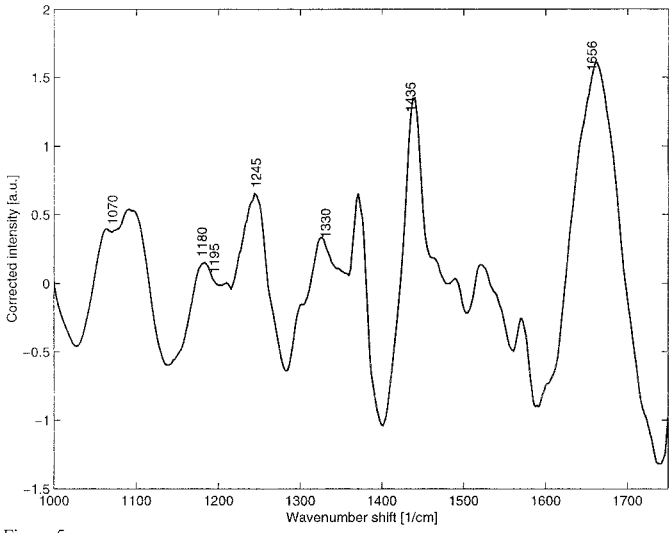

FIG. 5. Raman spectra of a suspension of cervical cancer cells.

dysplasia from all other samples with minimal classification errors. Similar algorithms were previously found to be useful in identifying high-grade squamous dysplasia in an *in vitro* study.[14]

The limitations of this study are that it is a pilot study with a small number of patients. Our experience shows that pilot studies are very useful in the development of emerging technologies; however, larger clinical trials are required to confirm these results. Improvements in hardware, measurement conditions, and training clinical staff to optimally participate in data collection are necessary to allow these larger trials. In particular, reducing the integration time and enabling measurements to be made under normal room lighting conditions would facilitate larger trials. Because these problems can be solved with increased excitation power and further optimized probe configurations,[25] Raman spectroscopy offers an attractive tool for surveying the biochemical changes that accompany the development of dysplasia.

1. T. J. Romer, J. F. Brennan, M. Fitzmaurice, M. L. Feldstein, G. Deinum, J. L. Myles, J. R. Kramer, R. S. Lees, and M. S. Feld, Circulation **97,** 878 (1998).
2. G. R. Gindi, C. J. Darken, K. M. O'Brien, M. L. Stetz, and L. I. Deckelbaum, IEEE T. Bio-Med Eng. **38,** 246 (1991).
3. D. L. Heintzelman, U. Utzinger, H. Fuchs, A. Gillenwater, R. Jacob, B. Kemp, and R. Richards-Kortum, Photochem. Photobiol. **72,** 103 (2000).
4. M. A. Mycek, K. T. Schomacker, and N. S. Nishioka, Gastrointest. Endosc. **48,** 390 (1998).
5. N. Ramanujam, M. F. Mitchell, A. Mahadevan-Jansen, S. L. Thomsen, G. Staerkel, A. Malpica, T. Wright, N. Atkinson, and R. Richards-Kortum, Photochem. Photobiol. **64,** 720 (1996).
6. R. Drezek, T. Collier, C. Brookner, A. Malpica, R. Lotan, and R. Richards-Kortum, Am. J. Obstet. Gynecol. **182,** 1135 (2000).
7. A. Zuluaga, M.S. Thesis, University of Texas at Austin (1998).
8. J. A. Swets, Science (Washington, D.C.) **240,** 1285 (1988).
9. M. F. Mitchell, S. B. Cantor, N. Ramanujam, G. Tortolero-Luna, and R. Richards-Kortum, Obstet. Gynecol. **93,** 462 (1999).
10. E. B. Hanlon, R. Manoharan, T. W. Koo, K. E. Shafer, J. T. Motz, M. Fitzmaurice, J. R. Kramer, I. Itzkan, R. R. Dasari, and M. S. Feld, Phys. Med. Biol. **45,** R1 (2000).
11. A. Mahadevan-Jansen and R. Richards-Kortum, J. Biomed. Opt. **1,** 31 (1996).
12. R. Manoharan, K. E. Shafer, L. Perelman, J. Wu, K. Chen, G. Deinum, M. Fitzmaurice, J. Myles, J. Crowe, R. R. Dasari, and M. S. Feld, Photochem. Photobiol. **67,** 15 (1998).
13. C. J. Frank, R. L. McCreery, and D. C. Redd, Anal. Chem. **67,** 777 (1995).
14. A. Mahadevan-Jansen, M. F. Mitchell, N. Ramanujam, A. Malpica, S. Thomsen, U. Utzinger, and R. Richards-Kortum, Photochem. Photobiol. **68,** 123 (1998).
15. C. J. de Lima, S. Sathaiah, L. Silveira, R. A. Zangaro, and M. T. Pacheco, Artif. Organs **24,** 231 (2000).
16. A. Mahadevan-Jansen, M. F. Mitchell, N. Ramanujam, U. Utzinger, and R. Richards-Kortum, Photochem. Photobiol. **68,** 427 (1998).
17. M. G. Shim, B. C. Wilson, E. Marple, and M. Wach, Appl. Spectrosc. **53,** 619 (1999).
18. T. F. Cooney, H. T. Skinner, and S. M. Angel, Appl. Spectrosc. **50,** 836 (1996).
19. T. F. Cooney, H. T. Skinner, and S. M. Angel, Appl. Spectrosc. **50,** 849 (1996).
20. J. E. Sansonetti, J. Reader, C. J. Sansonetti, and N. Acquista, J. Res. Natl. Inst. Stan. **97,** 1 (1992).
21. I. W. Selesnick and C. S. Burrus, IEEE T. Signal Proces. **46,** 1688 (1998).
22. A. Savitzky and M. J. E. Golay, Anal. Chem. **36,** 1627 (1964).
23. G. Deinum, D. Rodriguez, T. J. Romer, M. Fitzmaurice, J. R. Kramer, and M. S. Feld, Appl. Spectrosc. **53,** 938 (1999).
24. U. Utzinger, E. Vanessa Trujillo, E. N. Atkinson, M. F. Mitchell, S. B. Cantor, and R. Richards-Kortum, IEEE T. Bio-Med. Eng. **46,** 1293 (1999).
25. M. G. Shim, L. M. Song, N. E. Marcon, and B. C. Wilson, Photochem. Photobiol. **72,** 146 (2000).